Experimental Neurology 266 (2015) 74–85

Contents lists available at ScienceDirect

Experimental Neurology

journal homepage: www.elsevier.com/locate/yexnr

Regular Article

Focal transient CNS vessel leak provides a tissue niche for sequential immune cell accumulation during the asymptomatic phase of EAE induction☆

Deborah S. Barkauskas [a], R. Dixon Dorand [b], Jay T. Myers [a], Teresa A. Evans [c], Kestutis J. Barkauskas [d], David Askew [a], Robert Purgert [a], Alex Y. Huang [a,b,*]

[a] Division of Pediatric Hematology–Oncology, Department of Pediatrics, Case Western Reserve University School of Medicine, Cleveland, OH 44106, USA
[b] Department of Pathology, Case Western Reserve University School of Medicine, Cleveland, OH 44106, USA
[c] Department of Neurosciences, Case Western Reserve University School of Medicine, Cleveland, OH 44106, USA
[d] Department of Biomedical Engineering, Case Western Reserve University School of Engineering, Cleveland, OH 44106, USA

ARTICLE INFO

Article history:
Received 7 January 2015
Revised 3 February 2015
Accepted 11 February 2015
Available online 20 February 2015

ABSTRACT

Peripheral immune cells are critical to the pathogenesis of neurodegenerative diseases including multiple sclerosis (MS) (Hendriks et al., 2005; Kasper and Shoemaker, 2010). However, the precise sequence of tissue events during the early asymptomatic induction phase of experimental autoimmune encephalomyelitis (EAE) pathogenesis remains poorly defined. Due to the spatial–temporal constrains of traditional methods used to study this disease, most studies had been performed in the spine during peak clinical disease; thus the debate continues as to whether tissue changes such as vessel disruption represent a cause or a byproduct of EAE pathophysiology in the cortex. Here, we provide dynamic, high-resolution information on the evolving structural and cellular processes within the gray matter of the mouse cortex during the first 12 asymptomatic days of EAE induction. We observed that transient focal vessel disruptions precede microglia activation, followed by infiltration of and directed interaction between circulating dendritic cells and T cells. Histamine antagonist minimizes but not completely ameliorates blood vessel leaks. Histamine H1 receptor blockade prevents early microglia function, resulting in subsequent reduction in immune cell accumulation, disease incidence and clinical severity.

Introduction

Although disruption of CNS vessel integrity is a hallmark of MS, it is not clear whether such vascular compromise is the initiator or the result of the neuroinflammatory pathophysiology (Lassmann et al., 2007). Gross vascular compromises have been reported as an early onset indicator in the cerebellum and spine (Floris et al., 2004; Koh et al., 1993; Muller et al., 2005; Tonra et al., 2001). Current available data, however, does not adequately describe the nature and dynamics of the vessel leak. Previous studies on rats have shown: (1) via radiolabeling, that vessel leaks can be detected in the lower sacral region one day before clinical disease (Koh et al., 1993) and (2) via MRI, vessel leaks in the cerebellum and spine are detected by gadolinium on day 11 preceding macrophage infiltration and onset of clinical disease on day 14 (Floris et al., 2004). These observations are of major breaches in the vessel integrity, generally in the mm to cm size range. On the other hand, early vascular and associated tissue changes in the pre-symptomatic murine cerebral cortex undergoing EAE pathogenesis are less well defined.

The current dogma dictates that during EAE induction the blood–CNS barrier is rendered "leaky" by irradiation or pertussis toxin (PTx) through histamine-mediated effects (Linthicum et al., 1982). As engagement of H1R induces microglia activation (Dong et al., 2014), it is believed that microglia activation occurs during early EAE induction phase (Ponomarev et al., 2005). However, pathogenic T cell infiltration does not require microglial expression of the major histocompatibility antigen class II (MHCII) molecule (Greter et al., 2005), suggesting that another antigen-presenting cell (APC) subset, the dendritic cells (DCs), plays a crucial role in re-activating myelin-specific T cells in the CNS (Bailey et al., 2007). How circulating DC precursors are attracted to EAE lesions is not entirely clear.

Myelin-specific Th17 and Th1 T cells play critical roles in EAE and MS (Korn et al., 2009). Intravital two-photon microscopy (TPM) studies have examined the recruitment and behavior of pathogenic T cells in the mouse brain and spinal cord (Bartholomaus et al., 2009; Flügel et al., 2007; Herz et al., 2011; McGavern and Kang, 2011; Mues et al., 2013; Siffrin et al., 2010). These investigators focused their observation on T cell behavior during peak clinical symptomatic phase. As such,

☆ Conflict of interest: The authors declare no competing financial interests.

* Corresponding author at: Wolstein Research Building, Room 6528, 2103 Cornell Road, Cleveland, OH 44106-7288, USA.
E-mail address: alex.y.huang@case.edu (A.Y. Huang).

http://dx.doi.org/10.1016/j.expneurol.2015.02.018

these studies did not report how such T cells access the brain during the transition from the initiation stage to the infiltration stage of EAE pathogenesis (Lodygin et al., 2013; Odoardi et al., 2012; Sallusto et al., 2012). However, entry of T cells into the spinal cord in early EAE has been documented previously (Gordon et al., 2001; Kim et al., 2010; Rothhammer et al., 2011).

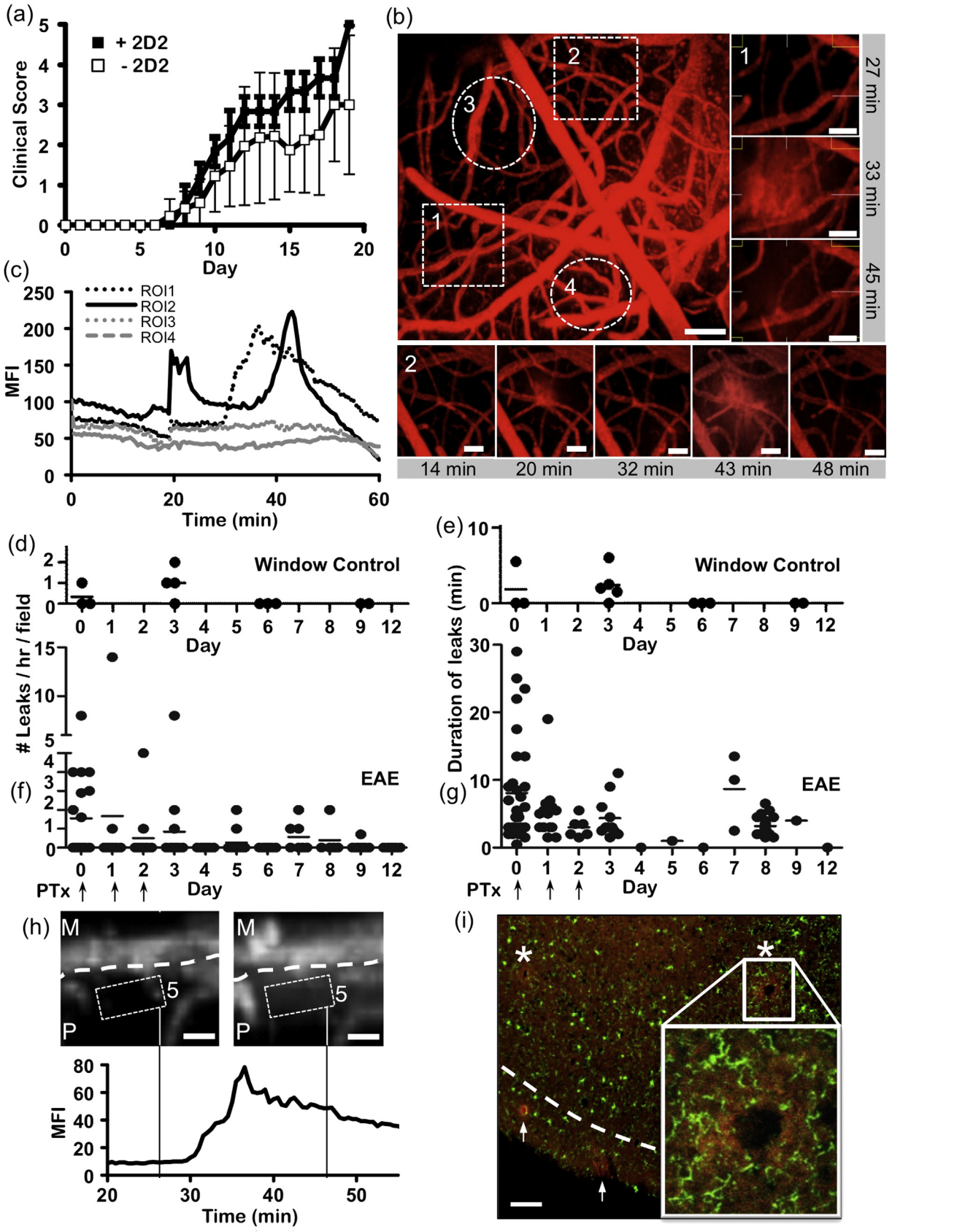

Here, we applied sequential TPM to examine cellular behavior at the tissue interface between the subarachnoid space (SAS) and cortex during the first 12 days of asymptomatic induction phase of EAE. We observed transient vessel leaks within the cortical gray matter within the first 3 days of disease induction, which initiated microglia activation, leading to sequential accumulation of DCs followed by myelin-specific T cell infiltration. We further showed that inhibiting histamine-induced microglia activation early in EAE induction could reduce disease progression. Specifically, we described early focal, intermittent and transient disruptions of post-capillary junctional venules following PTx administration, resulting in dextran uptake by the microglia, and immune cellular accumulation. Transient vessel leaks initiated an early parenchymal inflammatory response first evidenced by microglial uptake of blood contents, followed by an influx of both $CD11b^{+}CD11c^{+}$ and $CD11b^{+}CD11c^{-}$ APCs. The increasing numbers of activated CNS-resident and blood-derived APCs on days 3–6 facilitated the ingress and retention of activated T cells in a myelin-specific manner into the Virchow–Robin Space (VRS) and the parenchyma on days 6–12 before the clinical onset of disease. In contrast to other intravital imaging studies involving the spine, we focused our imaging effort on the cortex, which is relevant to human MS. Interestingly, a distinct pattern of immune cells congregated in patchy tissue niches that were in close proximity to sites of prior microvessel leaks. Early activation of CNS APCs and antigen recognition by T cells in the cortex subsequently affected the pattern of T cell migration in the cerebellum and spine. In addition, we show that histamine H1 receptor antagonist curtailed the frequency of PTx-induced focal vessel leakage, reduced the degree of microglia activation, diminished subsequent recruitment of circulating immune cells, and protected mice from EAE incidence and disease severity.

Materials and methods

Mice

2D2 (Bettelli et al., 2003) mice expressing the TCR transgene specific for MOG35–55 peptide/I-A^{b} (Jackson Labs, #006912) were crossed with B6.129 (ICR)-Tg actin-beta CFP mice (Jackson Labs, #004218) to derive mice expressing 2D2-CFP cells for in vivo tracking by TPM. Similarly, OTII mice expressing the TCR transgene specific for OVA323–339 peptide/I-A^{b} (Taconic, #1896) were crossed with C57BL/6-Tg ubiquitin GFP mice (Jackson Labs, #004353) to derive OTII-GFP cells for in vivo TPM tracking. C57BL/6J, B6.FVB-Tg CD11c-DTR/GFP mice (Jackson Labs, #004509) and B6.129P $CX_3CR1^{+/GFP}$ mice (Jackson Labs, #005582) were obtained from Jackson Laboratory. All animals were housed and handled in accordance with protocols approved by the CWRU IACUC.

Active EAE induction

EAE was actively induced in 8–12 week old female mice as previously described (Stromnes and Goverman, 2006). 3×10^{6} naïve splenic 2D2-CFP CD4 T cells, isolated by negative depletion using Dynal beads (Life Technologies, Grand Island, NY, USA) were injected into recipient mice. 24 h later, an emulsion with 200 μg myelin oligodendrocyte glycoprotein (MOG) peptide 35–55 (MOG35–55; AnaSpec, San Jose, CA, USA) with CFA (8 mg/mL H37RA and Incomplete Freund's Adjuvant (IFA); Difco Laboratories, Detroit, MI, USA) was injected subcutaneously (s.c.) bilaterally on the lower back of the recipient mouse (Hooke Laboratories, Lawrence, MA, USA). Control mice were injected s.c. bilaterally with an emulsion consisting of PBS and CFA. 100 ng pertussis toxin was administered intraperitoneal (i.p.) on days 0, 1 and 2. Daily clinical assessment of mice was performed. Clinical scores were assigned as previously described (Mi et al., 2007; Stromnes and Goverman, 2006).

Blood brain barrier leakiness analysis

To compare the pattern of vessel leakiness induced by different inflammatory stimulants, 100 ng LPS (Sigma-Aldrich, St. Louis, MO, USA), 100 ng PTx or 200 μL of PBS was injected i.p. into C57BL/6 mice on days 0, 1 and 2. 700 ng of 150 kDa TRITC dextran (Sigma-Aldrich, St. Louis, MO, USA) vessel dye was injected i.v. on day 1 and day 2. On day 3, QTracker-655 (Life Technologies, Grand Island, NY, USA) was injected to highlight the vessels. The mice were sacrificed and whole brain tissues were imaged immediately by TPM.

Priming of antigen-specific T cells

To determine whether myelin specific T cells require antigen-specific APCs for recruitment to the CNS, EAE was actively induced using a combination of two antigenic peptides in 8–12 week old female recipient mice. 3×10^{6} naïve 2D2-CFP and 3×10^{6} naïve OTII-GFP $CD4^{+}$ T cells were isolated separately by negative depletion using Dynal beads and co-injected into naïve recipient mice. 24 h later, an emulsion of 200 μg MOG35–55 only, 10 μg OVA323–339 only, or 200 μg MOG35–55 and 10 μg OVA323–339 combined (AnaSpec, San Jose, CA, USA) with CFA (8 mg/mL H37RA and IFA; Difco Laboratories, Detroit, MI, USA) was injected s.c. bilaterally on the lower back of the recipient mice. Control mice were injected s.c. bilaterally with an emulsion of PBS and CFA. 100 ng PTx (List Biological Laboratories, Inc., Campbell, CA, USA) was administered i.p. on days 0, 1 and 2 to induce EAE.

Flow cytometry analysis

For single-cell APC and T cell characterization, brain tissue was harvested on days 0 through 12 of EAE induction. Tissues were dissociated by collagenase D (1 mg/mL) and DNAse (250 units/mL) (Sigma-Aldrich, St. Louis, MO, USA) to form a single cell suspension after gentle dissociation with a dounce homogenizer and subjected to a 70%/37%/30% Percoll (Sigma-Aldrich, St. Louis, MO, USA) gradient (Cardona et al., 2006). Isolated cells were stained for CD45, CD11c, CD11b, CD4, CD8, IL-17, IFN-γ and FoxP3. Absolute numbers of cells per brain were determined by multiplying the number of events on FACS per collection volume by the total volume of cell samples. Spleen and LN were isolated from mice at the end of imaging on day 12. Organs were crushed with the ends of 1 mL syringes through a 40-μm cell strainer into single cell suspensions and were stained for Vα2 (OTII TCRα chain), Vβ11 (2D2 TCRβ chain), CD4, CD25, CD44, and CD69. Samples were collected and analyzed using the Accuri flow cytometer (BD Biosciences Co., San Jose, CA, USA).

Fig. 1. PTx administration caused early, transient and focal CNS vessel leaks. (a) Consistent clinical scores were achieved in mice pre-transferred with naïve 2D2 T cells (■; n = 6 from 2 experiments) as compared to non-transferred controls (□; n = 20 from 6 experiments) prior to EAE induction. (b) Dynamic TPM imaging of pial vessels (red) on day 3 after EAE induction. Scale bar = 50 μm. (c) Mean fluorescent intensity (MFI) measurements of the indicated ROIs in (b) over time revealed the transient and focal nature of the vessel leaks in ROIs 1 and 2. (d) Control mice with cranial window implantation and 7 days of recovery. (e) The duration of the leaks in (d) was short. There were no flares detected after day 3, up to 21 days. N = 4 from 1 experiment. (f) Frequency of cerebral vessel leaks was quantified by TPM during the first 12 days of EAE induction. Arrows: PTx injections. N = 19 from 8 independent experiments. (g) The duration of individual vessel leaks in (f) was measured dynamically by TPM. Arrows: PTx injections. (h) ROI 5 (a cross-sectional view of ROI 1 in (b)) revealed a slower clearance of vessel dye under the pial surface in the parenchyma (P) as compared to the meninges (M). Scale bar = 25 μm. (i) The presence of vessel dyes (red) can be detected by IHC in the perivascular areas of the CNS parenchyma in fixed $CX_3CR1^{+/GFP}$ brain tissue, both near the superficial vessels and the deep vessels away from the meningeal–parenchyma interface (*). Dash line: Imaging depth achieved by TPM. Scale bar = 100 μm. Data are shown as mean ± SD.

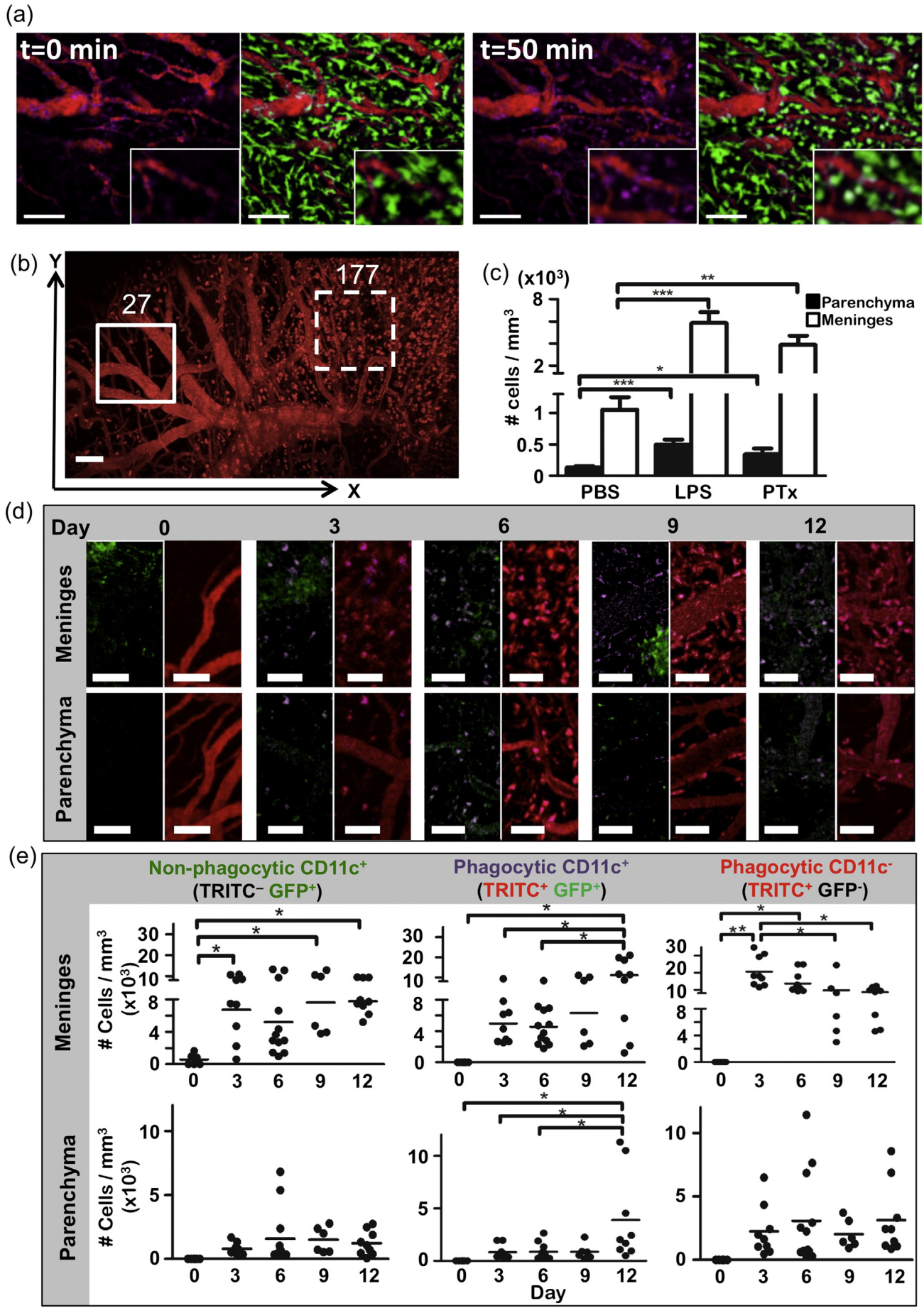
(a)
t=0 min
t=50 min
(b)
Y
X
27
177
(c)
(x10³)
cells / mm³
Parenchyma
Meninges
PBS
LPS
PTx
(d)
Day
0
3
6
9
12
Meninges
Parenchyma
(e)
Non-phagocytic CD11c⁺
(TRITC⁻ GFP⁺)
Phagocytic CD11c⁺
(TRITC⁺ GFP⁺)
Phagocytic CD11c⁻
(TRITC⁺ GFP⁻)
Meninges
Parenchyma
Cells / mm³
(x10³)
Day

Tissue histology analysis

After injection of TRITC vessel dye and completion of intravital imaging, $CX_3CR1^{+/GFP}$ mice were sacrificed and subjected to transcardial perfusion with 4% PFA. The brain tissue was harvested and 12-μm cryo-sections were performed and the samples were then subjected to confocal microscopy to obtain fluorescent images.

Intravital TMP imaging

Cranial windows were created as previously described (Mostany and Portera-Cailliau, 2008). The window surgery was performed 4 to 10 days before EAE induction to allow the local surgical site inflammation to subside. On the day of intravital imaging, 150 kDa TRITC dextran or QTracker 655 was injected i.v. 10 min prior to imaging to highlight the vasculature. Image acquisition was conducted using Leica SP5 microscope system on an upright DM6000 stage (Leica Microsystems, Inc.) fitted with a 20× (N.A. 1.0) water immersion lens. The SP5 microscope was coupled with a Ti/sapphire laser (16 W Chameleon XR laser, Coherent, Inc.) tuned to 880 nm to illuminate fluorescent elements within the live tissue. An image volume of 750 × 750 × 150 μm was routinely collected every 30 s to yield *xyzt* imaging data set.

Hydroxyzine treatment

Oral administration at 5 mg/kg/day was used for treatment with hydroxyzine. For the incidence curve, hydroxyzine was administered via drinking water at a concentration of 0.1 mM starting from day −1. Later, for FACS and TPM analyses, 5 mg/kg of hydroxyzine was administered via daily gavage from day −1 to day 12.

Imaging data analysis

Second harmonic generation (SHG) signal produced by high collagen content structures was used to identify the pial layer and to discriminate the parenchyma from meninges. Relative fluorescent intensity region of interest (ROI) measurements of dextran leaking into the parenchyma were made using the LAS-AF software (Leica Microsystems Inc., Buffalo Grove, IL, USA). Timing and duration of vessel leaks were manually processed. Cellular dextran uptake and CD11c-GFP were identified by fluorescent intensity. Co-localization of TRITC and GFP signals and volume data were calculated using the Imaris software (BitPlane Inc., Zurich, Switzerland). T cell motility data was also analyzed using the Imaris software, which allows cell identification, as well as 3D tracking over time by producing information on individual positions, time and track length. T cell interactions with APCs were grouped into short contacts (<2 min) and prolonged interactions (≥2 min). Individual T cell migration tracking was further analyzed for track length, velocity, mean fluorescent intensity and cell flux using MATLAB software (Mathworks Inc., Natick, MA, USA). Cell flux was calculated by determining the vector between the beginning of the T cell track and the point at which the T cell came within a 50-μm radius from the center of an APC cluster. Contact time between APC and T cells, and T cell movement to and from the blood vessel were analyzed manually by visual inspection of individual image slices over time using the Imaris software.

Statistical consideration

Statistical analyses were performed using GraphPad Prism 5 software (GraphPad Software Inc., San Diego, CA). For all analyses $p < 0.05$ was considered significant and degrees of freedom (df) are noted.

Results

Transient focal vessel leaks occurred early in EAE

EAE induction efficiency and clinical presentation can be variable. Therefore, to reliably capture rare cellular events by TPM we introduced fluorescent-labeled naïve 2D2 cells into recipient animals prior to disease induction in combination with a low dose of PTx on the first 3 days of induction without irradiation (Stromnes and Goverman, 2006). This resulted in 100% disease incidence compared to mice without transferred 2D2 cells (+2D2: n = 6 from 2 experiments; −2D2: n = 20 from 6 experiments), with hind limb paralysis achieved by day 21 (Fig. 1a). We focused our intravital observation in the cortex during the first 12 days of asymptomatic EAE induction (Luo et al., 2008). A cranial observation window was surgically implanted 4 to 10 days prior to induction in order to limit the inflammatory changes to structures and cellular response (Barkauskas et al., 2013; Dorand et al., 2014).

PTx has been shown to disrupt the BBB integrity in EAE (Linthicum et al., 1982), although the exact location, timing and dynamics of the vessel breach have not been carefully characterized to date. Using TPM and fluorescent-labeled vessel dye, we directly observed focal transient leakage of CNS vascular contents hours to days after PTx injections on days 0 to 2. These transient BBB breaches were visualized as blooms of dye leaking from the vessels (Fig. 1b; Movie 1). The effect of PTx on CNS vessel disruption was neither uniform nor permanent, as certain post-capillary venule junctions were prone to intermittent vessel leaks while other vessels of similar caliber remained completely intact (Fig. 1c). Control mice exhibited little to no vessel leaks (n = 4 from 1 experiment), indicating that these leaks were not due to damages associated with TPM or prior surgical procedures (Figs. 1d and e). Furthermore, we observed vessel leaks that originated from the vessels outside of the imaging field, arguing against this phenomenon as an artifact of TPM (Movie 2). When the vessel leaks were serially characterized in the same mice through the first 12 days of EAE induction, we observed the highest frequency of vessel leaks during the first 3 days (n = 19 from 8 experiments), coincident with PTx administration (Fig. 1f). The duration of individual leaks during this early period was variable, with some lasting ~30 min before resolving (Fig. 1g). While vessel content quickly dissipated at the pial surface by the bulk CSF flow in the meningeal space, blood solutes released into the parenchyma took a longer time to clear after resolution of the BBB breach (Fig. 1h). Evidence of blood persistence can be found deep in the parenchyma, as TRITC-labeled dextran was observed on day 3 in fixed brain tissue (Fig. 1i).

Identity of $TRITC^+$ cells in early EAE

Next, we examined the focal and intermittent nature of the vessel breach by measuring the location and the dextran uptake activity in the cortex throughout EAE induction. CX_3CR1 is constitutively expressed by the microglia and a sub-population of macrophages in the CNS (Kettenmann et al., 2011). To identify the $TRITC^+$ cells, we

Fig. 2. Focal vessel leaks induced localized activation of endogenous CNS immune cells and accumulation of DCs. (a) Day 0 after EAE induction showed that all $TRITC^+$ cells (red) were confined within $CX_3CR1^{+/GFP}$ (green) cells. (b) TPM vessel imaging of the cortex on day 3 following PTx administration revealed aggregates of $TRITC^+$ cells (red) while other similarly imaged areas were devoid of pinocytic activities. The numbers indicate dextran-laden cell counts within the boxed parenchymal volume. Scale bar = 100 μm. (c) Quantification of $TRITC^+$ cells in the meninges and parenchyma following systemic exposure to LPS and PTx. $^*p < 0.01$, $^{**}p < 0.001$, $^{***}p < 0.0001$. PBS, n = 7; PTx, n = 6; LPS, n = 4 from 2 independent experiments. (d) Sequential CNS imaging of the CD11c-GFP mice over the first 12 days of EAE induction showed progressive changes in the accumulation of $CD11c^+$ (green) and $TRITC^+$/$CD11c^+$ (purple) cells in the left panel and $TRITC^+$ only cells (red) in the right panel over time. Scale bar = 60 μm. (e) Quantification of $CD11c^+$ (green), $TRITC^+$/$CD11c^+$ (purple) and $TRITC^+$ (red) cells in the meninges and parenchyma over a 12-day sequential imaging experiment as shown in (d). N = 5 mice from 2 independent experiments. Data are shown as mean ± SD.

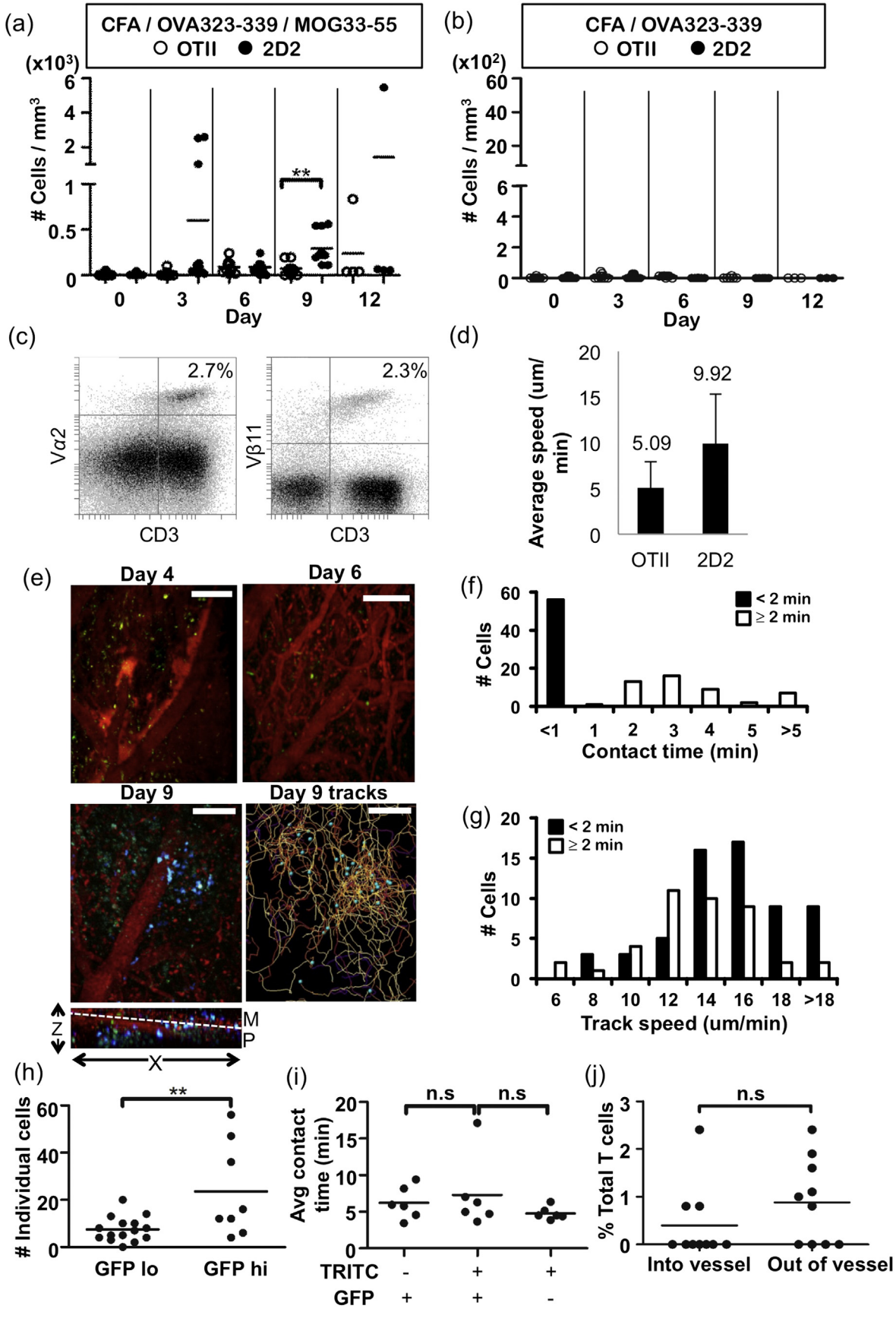
(a)
CFA / OVA323-339 / MOG33-55
OTII 2D2
(x10³)
Cells / mm³
Day
**
(b)
CFA / OVA323-339
OTII 2D2
(x10²)
Cells / mm³
Day
(c)
2.7%
2.3%
Vα2
Vβ11
CD3
CD3
(d)
Average speed (um/min)
9.92
5.09
OTII
2D2
(e)
Day 4
Day 6
Day 9
Day 9 tracks
Z
M
P
X
(f)
Cells
< 2 min
≥ 2 min
Contact time (min)
(g)
Cells
< 2 min
≥ 2 min
Track speed (um/min)
(h)
Individual cells
**
GFP lo
GFP hi
(i)
Avg contact time (min)
n.s
n.s
TRITC
GFP
(j)
% Total T cells
n.s
Into vessel
Out of vessel

induced EAE in *Cx3cr1*$^{+/GFP}$ mice. Five hours after PTx administration on day 0, the only TRITC$^+$ cells in the meninges and parenchyma were 100% CX$_3$CR1$^+$ cells (Fig. 2a).

Intermittent vessel leaks resulted in localized uptake of blood vessel contents by the microglia

When TRITC-labeled dextran was introduced intravenously on 3 consecutive days during PTx administration, we observed a patchy distribution of TRITC-labeled cells throughout the parenchyma, while other areas within the same imaging field have little to no detectable TRITC-labeled cells (Fig. 2b). The distribution of TRITC$^+$ cells is consistent with the distribution pattern of transient vessel leaks observed in Fig. 1. Serial imaging of the same CNS location also revealed that the vessel leaks coincided with observed increase in the TRITC–dextran uptake and activation of the nearby microglia, as judged by morphologic changes (Fig. 2a, inset), thereby starting a cellular cascade that results in the infiltration and accumulation of circulating immune cells.

Toxin-dependent phagocytic activation

To assess how the phagocyte distribution may be affected by neuroinflammatory stimuli, we compared the distribution and numbers of TRITC$^+$ cells following systemic exposure to PTx and the TLR4 agonist, lipopolysaccharide (LPS). We observed a distinct distribution pattern of parenchymal TRITC$^+$ cells between the two stimuli: systemic LPS produced an even distribution of TRITC$^+$ cells throughout the entire parenchyma and meninges, whereas PTx treatment resulted in a patchy TRITC$^+$ distribution (data not shown) as seen with EAE induction (Fig. 2b). Both PTx and LPS administration resulted in a significant increase in the appearance of TRITC$^+$ cells in both the meninges (PTx, $df = 11$, $p = 0.0082$; LPS, $df = 8$, $p = 0.0004$) and parenchyma (PTx, $df = 11$, $p = 0.046$; LPS, $df = 8$, $p = 0.0009$) (Fig. 2c; two-tailed unpaired t-test). This method allows serial documentation of the vessel leak patterns in the same hosts with finer time and space resolution than previously reported (Findling et al., 1994).

CD11c$^+$ DCs infiltrate the CNS following phagocyte activation

CD11c$^+$ DCs are required in EAE induction (Bailey et al., 2007; Miller et al., 2007). To determine the time course of infiltrating DCs and their phagocytic activities in the CNS, we imaged CD11c-GFP$^+$ mice daily during the first 12 days of active EAE induction (Fig. 2d). We quantified the number of CD11c-GFP$^+$ cells, TRITC$^+$ cells, or both in the meninges and parenchyma (Fig. 2e; 1 way ANOVA with $df = 41$). We observed a significantly increased number of CD11c$^+$TRITC$^-$ cells in the meninges starting on days 3 through 12, with increasing dextran uptake from days 9 to 12. The entry of CD11c$^+$TRITC$^-$ DCs into the parenchyma was much slower compared to those in the meninges, with DCs increasing in number starting on day 6. Their phagocytic capacity increases over the subsequent 6 days. In contrast, the number of CD11c$^-$ TRITC$^+$ cells in the meninges decreased between days 3 to 12, even as parenchymal CD11c$^-$ TRITC$^+$ cell numbers remain constant throughout this period.

Presentation of myelin antigens by CNS APCs enhanced activated myelin-specific T cell entry and retention

Following the characterization of CD11c$^+$ and CD11c$^-$ APCs in the EAE brain, we investigated the timing and antigen requirement of 2D2 cell recruitment and behavior within the CNS. More 2D2 cells began to infiltrate the brain parenchyma on day 3 and significantly more on day 9 (Fig. 3a; $n = 5$ from 2 experiments, $df = 8$, $p = 0.0082$, 1 way ANOVA). However, when mice adoptively transferred with naïve OTII and 2D2 cells were immunized only with OVA323–339, we saw a near complete absence of infiltrating 2D2 or OTII cells in the meninges or the CNS parenchyma (Fig. 3b), even though both T cell populations were found in equivalent numbers within the peripheral lymph nodes (Fig. 3c). The few OTII cells resided only transiently in the CNS next to blood vessels and migrated with a reduced speed as compared with 2D2 cells (Fig. 3d). The divergent behaviors between the two T cell populations were observed in the presence of equivalent leaky CNS vessels, phagocytic APC accumulation and robust T cell activation within the same host. Taken together, our data imply that the cooperation between PTx-induced leaky vessels, resident and infiltrating APCs, the availability of CNS-derived antigens and activated myelin-specific T cells are preconditions for MOG-specific T cell entry into the CNS, which in turn amplifies other cellular infiltration later in the disease progression.

Localized blood vessel leaks preceded phagocyte accumulation and the infiltration of DCs and T cells

To further examine the cellular and structural cooperation leading to EAE, we performed multiplex sequential imaging to capture cellular interactions among TRITC$^+$ cells, DCs and 2D2 cells during the first 9 days of EAE induction. Following transient vessel leaks (Fig. 3e, day 4), the vessel content was cleared with a concomitant increase in the number of TRITC$^+$ cells and the arrival of CD11c$^+$ DCs by day 6 (Fig. 3e, days 6–9). This was followed on day 9 by a large number of infiltrating 2D2 cells that congregated near sites of previous vessel leaks (Fig. 3e, day 9), eventually leading to extensive inflammatory changes, with tail and limb weakness beginning on days 10 onward (Fig. 1a). The 2D2 cells surveyed a large parenchymal area, while maintaining focal movements surrounding sites of prior vessel leak where clusters of CD11c$^+$ cells were also found (Fig. 3e, day 9 tracks; Movie 3). The 2D2 cells exhibited both transient (<2 min) and prolonged (≥2 min) contacts with DCs (Fig. 3f). Those 2D2 cells that interacted briefly with CD11c$^+$ DCs migrated at faster velocities (~14.8 ± 4.2 μm/min), while those that exhibited prolonged interaction with DCs traveled with reduced velocities (~12.5 ± 3.6 μm/min) (Fig. 3g). In all, 83% of 2D2 cells were motile, with 6.1 ± 5.1% of 2D2 cells residing in the perivascular areas with limited motility.

2D2 cells preferentially congregated in DC-rich regions

To assess whether 2D2 cells were preferentially drawn to sites of DC aggregates, we analyzed the number of 2D2 cells entering a 50-μm radius of a CD11c$^+$-GFP$^+$ cellular aggregate. Our analysis revealed a significant increase in the number of unique 2D2 cells moving toward an area high in GFP signals as compared to areas with low GFP signals within

Fig. 3. Peripherally activated T cells accumulated and migrated near sites of vessel leak and DC aggregation in an antigen-dependent manner. (a) Direct TPM observation of naïve OTII and 2D2 co-transferred mice that were immunized with both OVA323–339 and MOG35–55 peptides in the presence of CFA and PTx. N = 5 from 2 independent experiments. (b) TPM observation of naïve OTII and 2D2 co-transferred mice that were immunized with only the OVA323–339 peptide. N = 3 from 1 experiment. (c) Flow cytometry analysis of OTII (Vα2) and 2D2 (Vβ11) cells in the peripheral draining lymph nodes of mice in (a). (d) Comparison of the average migration speeds of OTII and 2D2 cells found in the brain. (e) Sites of focal vessel leaks early in EAE induction (day 4) resulted in TRITC$^+$ (red) and CD11c-GFP$^+$ (green) cell accumulation (days 6–9), along with localized 2D2 cell (blue) migration and accumulation (day 9). Colored tracks on day 9 highlight the paths taken by individual 2D2 cells (blue) near areas of CD11c-GFP$^+$ cell clusters (green) in the parenchyma (P) compared to the meninges (M). (f) Contact duration of CD11c-GFP$^+$ cells by 2D2 T cells on day 9. (g) Average velocity of 2D2 cells based on interaction times. (h) Total number of unique 2D2 cells migrating toward CD11c$^+$ rich regions (GFP^{hi}) versus low CD11c-GFP (GFP^{lo}) regions on days 9 and 12. N = 5 from 2 independent experiments. (i) 2D2 cells exhibited similar overall contact time with APCs on days 9 and 12. N = 5 from 2 independent experiments. (j) More 2D2 cells egressed from the blood vessels into the parenchyma as compared to those entering into the blood vessels from the CNS on days 9 and 12. N = 5 from 2 independent experiments. $^{**}p < 0.001$; n.s., not significant. Data are shown as mean ± SD.

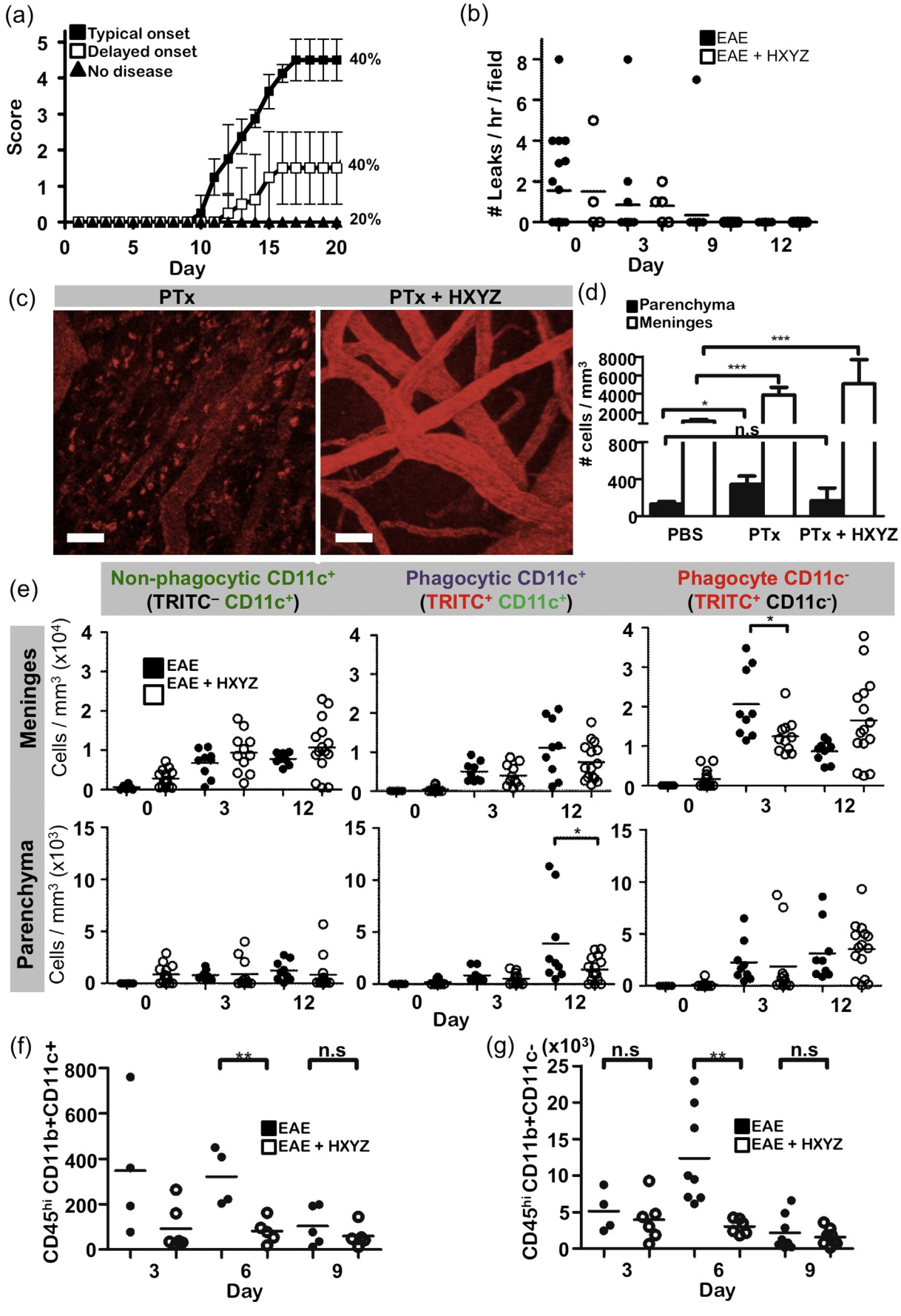
(a)
Typical onset
Delayed onset
No disease
Score
Day
40%
40%
20%
(b)
EAE
EAE + HXYZ
Leaks / hr / field
Day
(c)
PTx
PTx + HXYZ
(d)
Parenchyma
Meninges
cells / mm3
n.s
PBS
PTx
PTx + HXYZ
(e)
Non-phagocytic CD11c+
(TRITC− CD11c+)
Phagocytic CD11c+
(TRITC+ CD11c+)
Phagocyte CD11c-
(TRITC+ CD11c-)
Meninges
Parenchyma
Cells / mm3 (x10^4)
Cells / mm3 (x10^3)
EAE
EAE + HXYZ
Day
(f)
CD45hi CD11b+CD11c+
n.s
EAE
EAE + HXYZ
Day
(g)
CD45hi CD11b+CD11c- (x10^3)
n.s
EAE
EAE + HXYZ
Day

the same imaging field (Fig. 3h; n = 5 from 2 experiments, df = 21, p = 0.0069, two-tailed unpaired t-test). Contact duration analysis of 2D2 cells with $CD11c^+$ and $CD11c^-$ phagocytes showed a trend toward longer duration of contact with $CD11c^+$ cells (Fig. 3i; n = 5 from 2 experiments, df = 17, p value not significant, 1 way ANOVA). We also found a trend for a greater number of 2D2 cells egressing from nearby blood vessels to enter the $CD11c^+$ rich regions as compared to those entering the vessels from the parenchyma (Fig. 3j; Movies 4, 5; n = 5 from 2 experiments, df = 24, p value not significant, two-tailed unpaired t-test).

Histamine H1 receptor blockade reduced microglia activation, DC recruitment, disease incidence and clinical severity

Histamine released by mast cells is implicated in PTx-mediated vessel leak (Linthicum et al., 1982). We tested whether blockade of the histamine H1 receptor (H1R) could ameliorate observed vessel leak and subsequent cellular accumulation events. We administered hydroxyzine (HXYZ), a H1R antagonist that readily crosses the BBB, in the drinking water of mice undergoing EAE induction. We observed a 60% reduction in EAE incidence among mice receiving HXYZ treatment (Fig. 4a; n = 10 from 2 experiments). Despite HXYZ treatment via gavage, however, we still observed PTx-induced vessel leaks (Figs. 4b, c; Movie 6). Nevertheless, HXYZ treatment did result in a dramatic reduction in the number of $TRITC^+$ parenchymal cells, with numbers comparable to PBS control (Fig. 4d; PBS: PTx + HXYZ, df = 7, p value not significant, two-tailed unpaired t-test). These findings were further corroborated by TPM, showing a trend toward reduction of $TRITC^+$ cells and DCs as late as day 12 (Fig. 4e, day 3; df = 18, p = 0.0146; day 12 df = 22, p = 0.0386; two-tailed unpaired t-test). Flow cytometry analysis revealed a reduction in the number of both $CD11b^+CD11c^+$ DCs (Fig. 4f; df = 7, p = 0.006, two-tailed unpaired t-test) and $CD11b^+$-$CD11c^-$ macrophages (Fig. 4g; df = 12, p = 0.0049, two-tailed unpaired t-test), as well as a similar reduction in the number of infiltrating $CD8^+$ (Fig. 5a; df = 8, p = 0.0013, two-tailed unpaired t-test) and $CD4^+$ T cells (Fig. 5b; df = 8, p = 0.0005, two-tailed unpaired t-test) in HXYZ-treated groups early on day 3. This was accompanied by a reduced number of CNS infiltrating IL-17 and IFN-γ producing $CD4^+$ T cells (Fig. 5c, day 9; IL-17: df = 8, p = 0.036; IFN-γ: df = 8, p = 0.024; two-tailed unpaired t-test), even though the spleens of these mice contained similar numbers of IL-17 and IFN-γ producing $CD4^+$ T cells (Fig. 5d).

Discussion

CNS vessel leak has been implicated as a trigger in neurodegenerative disorders including epilepsy, Alzheimer, and Parkinson's disease (Hawkins and Davis, 2005; Zlokovic, 2011). Although changes in CNS vessel permeability have been documented in vivo, the timing and kinetics at the level of detail as described in the current study has not been reported previously (Davalos et al., 2012; Findling et al., 1994; Kenne and Lindbom, 2011; McGavern and Kang, 2011). We provided evidence of the transient and focal nature of altered vascular permeability in early EAE induction as an initiating event, not a byproduct of effector T cell aggregation and tissue destruction near the perivascular pathologic lesions. These leaks occurred during PTx treatment, where blood contents including plasma proteins and fibrinogen (Davalos et al., 2012) are released into the parenchyma and initiate a parenchymal inflammatory response including the activation of the phagocytic capacity of resident CX_3CR1^+ microglia (Neumann et al., 2009), well in advance of any observable clinical symptoms. Vessel leaks were found in the meninges and throughout the parenchyma. During the early vessel leaks following PTx administration, we did not detect influx of circulating monocytes or T cells in the cortex, suggesting that the opening of the BBB at this stage does not permit a large influx of circulating cells into the imaged region of the brain. At later time points (days 4–6) when the vessel leakage subsides, we began to observe increasing immune cell infiltrate coincident with a second wave of vessel leak (Figs. 1d, e; days 7–9), an observation consistent with the two-step paradigm of EAE induction (Sallusto et al., 2012). Interestingly, while PTx administration resulted in focal dextran-uptake activity, systemic administration of LPS, the classical TLR4 agonist, resulted in a diffuse pattern of dextran uptake in the CNS presumably due to the direct effect of LPS on endothelial and immune cells throughout the body (Andonegui et al., 2003, 2009). The observed differential effects between PTx and LPS on CNS dextran uptake are interesting, since PTx has been shown to evoke intracellular signaling through TLR4 (Kerfoot et al., 2004).

Mice with functionally deficient microglia exhibited delayed EAE onset and reduced severity, suggesting microglia contribution in EAE pathogenesis (Greter et al., 2005; Heppner et al., 2005). Peritoneal macrophages activated with ConA display increased pinocytosis concomitant with an increase in phagocytosis, and prolonged pinocytosis may be an indicator of macrophage activation (Cohn, 1966). Depending on the mode of activation, however, pinocytosis may also decrease as compared to non-activated macrophages (Montaner et al., 1999; Tsang et al., 2000). Pinocytosis is a highly metabolic process and requires an ATP source such as dextran (Edelson et al., 1975). In our study, we found that the microglia surrounding the vessel leaks were pinocytic. Using the $CX_3CR1^{+/GFP}$ reporter mouse, we showed that the microglia and macrophages constitute the main pinocytic populations that absorb vessel contents in the first 3 days. These cells can internalize vessel contents in response to TLR agonist stimulation by one of two ways. First, they act as scavengers, removing blood solutes following vessel leaks. Second, perivascular CX_3CR1^+ cells can sample blood contents directly within intact blood vessels through intravascular processes (Barkauskas et al., 2013).

Bone marrow derived myeloid cells are also important in regulating CNS inflammatory response, where infiltrating DCs with functional MHCII are required for EAE induction (Bailey et al., 2007; Greter et al., 2005; Heppner et al., 2005; Juedes and Ruddle, 2001; Miller et al., 2007; Pashenkov et al., 2003; Serafini et al., 2000). Activated OTII cells can access the CNS only in the presence of co-activated 2D2 cells. In contrast, activated OTII cells in the presence of naïve 2D2 cells were incapable of doing so, despite the presence of pinocytic microglia and DCs. These results suggest that T cells do not simply enter CNS passively through disrupted BBB but require activated 2D2 cells recognizing myelin-presenting APCs. Our data support the view that APCs presenting endogenous CNS peptides are critical to license T cell recruitment and retention in the EAE brain. Our TPM imaging and FACS data are in good agreement with reports showing that 5–10% of $CD11b^+$ cells

Fig. 4. Histamine receptor blockade inhibited early activation of CNS $TRITC^+$ cells, diminished DC and 2D2 cell accumulation, and blunted EAE severity. (a) 60% of mice displayed absent or reduced severity of disease when exposed to hydroxyzine (HXYZ) via drinking water during EAE induction, with 20% disease-free incidence and 40% with a delayed onset and reduced overall clinical severity. N = 10 per group from 2 independent experiments. (b) Frequency of CNS vessel leaks was observed by direct TPM observation after HXYZ was administered to mice via gavage followed by EAE induction. No statistical differences in vessel leaks were observed in HXYZ-gavaged mice as compared to control mice during EAE induction. N = 6 per group from 2 independent experiments. (c) EAE-induced mice treated with HXYZ showed a dramatic reduction in $TRITC^+$ cells. Scale bar = 50 μm. (d) Cell number in both meninges and parenchyma with PTx treatment versus PTx + HXYZ treated as compared to PBS controls. PBS, n = 7; PTx, n = 6; PTx + HXYZ, n = 4 from 2 independent experiments. (e) Sequential TPM imaging data analysis of HXYZ-treated and control mice showed a substantial decrease in parenchymal and meningeal $CD11c^+$ and $CD11c^-$ $TRITC^+$ numbers during EAE induction between days 3 and 12. HXYZ-treated, n = 6; control, n = 5 from 2 independent experiments. (f) After whole brain Percoll isolation of cells from HXYZ-treated and control mice, flow cytometry analysis revealed a significant decrease in the number of $CD11b^+CD11c^+$ cells in the CNS of HXYZ-treated mice on days 3 and 6 following EAE induction. N = 8 from 2 independent experiments. (g) The number of $CD11b^+CD11c^-$ cells in the CNS of HXYZ-treated mice was also significantly lower as compared to control on day 6 following EAE induction. N = 8 from 2 independent experiments. Data are shown as mean ± SD. *p < 0.01; **p < 0.001; ***p < 0.0001; n.s., not significant.

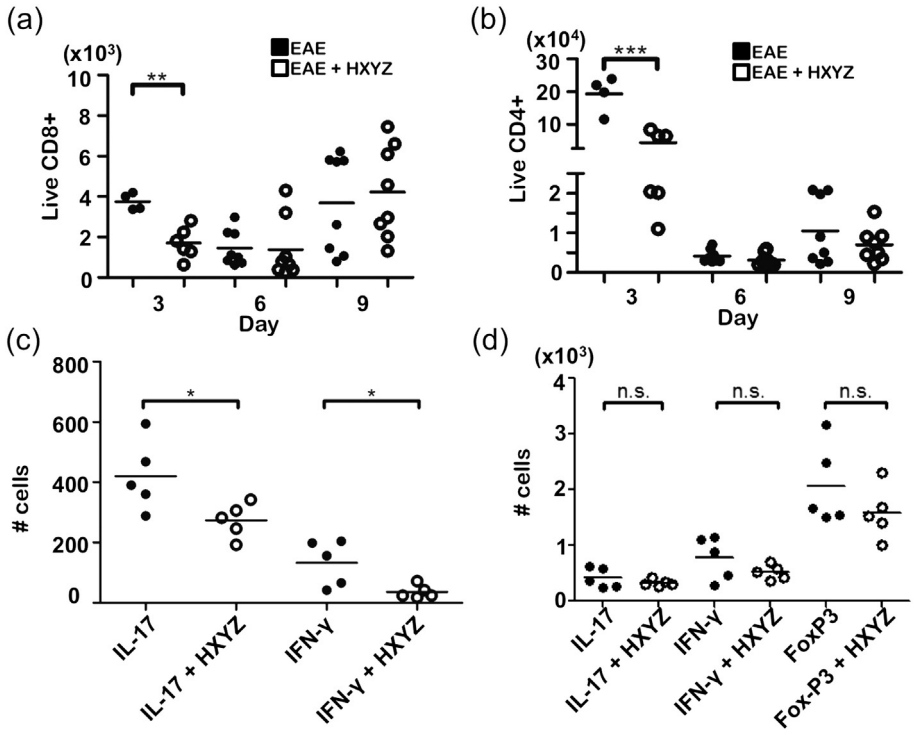

Fig. 5. Effects of HXYZ on T cell numbers during EAE induction. HXYZ was administered via gavage from day −1 to day 12 while EAE was being induced. Whole-brain Percoll isolations of individual cells from HXYZ-treated and control mice were performed. Flow cytometry analysis of the isolated cells showed the following: (a) a significant decrease in the number of $CD8^+$ cells in the CNS with HXYZ treatment on day 3. N = 8 from 3 independent experiments. (b) A significant decrease in the number of $CD4^+$ cells in the CNS with HXYZ treatment on day 3. N = 8 from 3 independent experiments. (c) Although the total number of $CD4^+$ cells in the CNS was similar between treatment and control groups (b) on day 9, there was a significant decrease in the number of IFN-γ and IL-17 producing cells within the CNS. N = 5 from 2 independent experiments. (d) The total number of $CD4^+$ T cells expressing IFN-γ, IL-17 and FoxP3 was not significantly different with HXYZ treatment on day 9 in the spleen. N = 5 from 2 independent experiments. *$p < 0.01$; **$p < 0.001$; ***$p < 0.0001$; n.s., not significant.

present myelin basic protein as early as day 1 after EAE induction, whereas $CD11c^+$ DCs are not detected till after day 5 and only present myelin basic protein from day 7 onwards (Sosa et al., 2013).

T cell infiltration into the brain was thought to only occur at the choroid plexus, although recent data suggest an alternate route via VRS and the pial vessels in the SAS (Goverman, 2009; Ransohoff and Engelhardt, 2012). Our imaging data captured T cells migrating directly into the parenchyma from VRS, and migrated near $CD11c^+$ DCs in a pattern that were in contrast to published data showing non-directed T cell behavior during the peak of EAE disease (Bartholomaus et al., 2009; Herz et al., 2011; McGavern and Kang, 2011; Mues et al., 2013; Siffrin et al., 2010). Our finding of the focal T cell accumulation and their repeated surveillance with DCs during the asymptomatic phase of EAE suggests direct communication between newly arrived 2D2 and DCs. These short contacts were similar to other reports, which utilized calcium flux and NFAT reporter mice to show that infiltrating T cells in the spine of passively induced EAE mice were in an activated state while meandering and making short contacts with phagocytic APCs (Lodygin et al., 2013; Mues et al., 2013). Here, we showed that 2D2 cells are re-activated by DCs in the cortex before these T cells exert their pathogenic effector function, eventually leading to the development of clinical symptoms.

PTx has been shown to increase the permeability of vessels (Linthicum et al., 1982; Locht et al., 2011; Miyata and Morita, 2011) with direct effects on the choroid plexus and cerebral endothelial cells (Brückener et al., 2003; Lapilla et al., 2011). In the brain, PTx is postulated to act through histamine, which causes vasodilation, changes adhesion molecule expression, and alters endothelial tight junctions and astrocyte end feet barrier integrity. Mice deficient in histamine receptors 1 and 2 have reduced EAE severity and BBB permeability (Saligrama et al., 2012). The CSF of MS patients contains elevated levels of histamine, and H1R antagonists have shown clinical benefits in MS (Jadidi-Niaragh and Mirshafiey, 2010). In a clinical trial, hydroxyzine was shown to stabilize or improve symptoms in 75% of MS patients (Logothetis et al., 2005).

Interestingly, we only observed a trend toward diminished frequency, but not a complete absence of vessel leakage when HXYZ was administered. Our observation suggests that mechanism(s) other than histamine are responsible for vessel permeability changes under neuroinflammatory conditions, such as tachykinins (e.g. substance P), serotonin, and bradykinin (Annunziata et al., 1998, 2002; Feng et al., 1996; Kakizoe et al., 1997; Olesen, 1985; Reinke et al., 2006; Saria et al., 1983). Regardless, we showed that HXYZ treatment reduced EAE disease incidence or severity in 60% of the mice. Furthermore, HXYZ initially reduced the extent of dextran uptake by meningeal macrophage as documented by TPM and decreased the myeloid-derived APC infiltration globally in the CNS. Importantly, preventing the early activation of the microglia with HXYZ resulted in a reduction of both non-specific T cell infiltration on day 3 and antigen-specific T cell infiltration on day 12. These data provide further evidence supporting the view that the microglia play critical roles in early EAE induction, and that blocking microglia activation during the inflammatory phase can lessen myelin and neuronal destruction (Giunti et al., 2013; Juedes and Ruddle, 2001; Saijo and Glass, 2011). Future work remains to fully understand the regulation of focal and intermittent CNS vessel disruption that was only partially blocked by H1R blockade.

The exact kinetics of cellular inflammation in the brain have been hard to study, especially during the very early stages of EAE induction prior to disease manifestation, due to the low number of relevant cells detected using conventional bulk cellular assays. Our present study helps to shed new light on the precise, local and sequential interplay among CNS tissues and cellular factors that coordinately manifest in early EAE pathophysiology involving early intermittent BBB disruption, local activation of the microglia, subsequent recruitment of DCs, and the surveillance behavior of pathogenic $CD4^+$ T cells in the EAE brain.

Supplementary data to this article can be found online at http://dx.doi.org/10.1016/j.expneurol.2015.02.018.

Acknowledgments

We thank the following for discussion and critique on this work: R. Ransohoff, F. Scrimieri, T. Welliver, A. Tong, A. Petrosiute, J. Tsai, E. Bays, and Y. Othman. This work was supported by NIH EB007509 (D.S.B.), NIH GM007250 (R.D.D.), the Wolstein Research Scholarship (R.D.D.), NIH GM007250 (T.A.E.), NIH R00EB011527 (K.J.B.), the Steven G. Giallourakis AYA Cancer Research Foundation (D.A., R.P.), the Dana Foundation, the Gabrielle's Angels Foundation (217487, 104927), the St. Baldrick's Foundation, the Hyundai "Hope-on-Wheels" Program and the Alex's Lemonade Stand Foundation (A.Y.H.).

References

Andonegui, G., Bonder, C.S., Green, F., Mullaly, S.C., Zbytnuik, L., Raharjo, E., Kubes, P., 2003. Endothelium-derived Toll-like receptor-4 is the key molecule in LPS-induced neutrophil sequestration into lungs. J. Clin. Invest. 111, 1011–1020.

Andonegui, G., Zhou, H., Bullard, D., Kelly, M.M., Mullaly, S.C., McDonald, B., Long, E.M., Robbins, S.M., Kubes, P., 2009. Mice that exclusively express TLR4 on endothelial cells can efficiently clear a lethal systemic Gram-negative bacterial infection. J. Clin. Invest. 119, 1921–1930.

Annunziata, P., Cioni, C., Toneatto, S., Paccagnini, E., 1998. HIV-1 gp120 increases the permeability of rat brain endothelium cultures by a mechanism involving substance P. AIDS 12, 2377–2385.

Annunziata, P., Cioni, C., Santonini, R., Paccagnini, E., 2002. Substance P antagonist blocks leakage and reduces activation of cytokine-stimulated rat brain endothelium. J. Neuroimmunol. 131, 41–49.

Bailey, S.L., Schreiner, B., McMahon, E.J., Miller, S.D., 2007. CNS myeloid DCs presenting endogenous myelin peptides 'preferentially' polarize CD4+ T(H)-17 cells in relapsing EAE. Nat. Immunol. 8, 172–180.

Barkauskas, D.S., Evans, T.A., Myers, J., Petrosiute, A., Silver, J., Huang, A.Y., 2013. Extravascular CX3CR1+ cells extend intravascular dendritic processes into intact central nervous system vessel lumen. Microsc. Microanal. 19, 778–790.

Bartholomaus, I., Kawakami, N., Odoardi, F., Schlager, C., Miljkovic, D., Ellwart, J.W., Klinkert, W.E., Flugel-Koch, C., Issekutz, T.B., Wekerle, H., Flugel, A., 2009. Effector T cell interactions with meningeal vascular structures in nascent autoimmune CNS lesions. Nature 462, 94–98.

Bettelli, E., Pagany, M., Weiner, H.L., Linington, C., Sobel, R.A., Kuchroo, V.K., 2003. Myelin oligodendrocyte glycoprotein-specific T cell receptor transgenic mice develop spontaneous autoimmune optic neuritis. J. Exp. Med. 197, 1073–1081.

Brückener, K.E., el Bayâ, A., Galla, H.J., Schmidt, M.A., 2003. Permeabilization in a cerebral endothelial barrier model by pertussis toxin involves the PKC effector pathway and is abolished by elevated levels of cAMP. J. Cell Sci. 116, 1837–1846.

Cardona, A.E., Huang, D., Sasse, M.E., Ransohoff, R.M., 2006. Isolation of murine microglial cells for RNA analysis or flow cytometry. Nat. Protoc. 1, 1947–1951.

Cohn, Z.A., 1966. The regulation of pinocytosis in mouse macrophages. I. Metabolic requirements as defined by the use of inhibitors. J. Exp. Med. 124, 557–571.

Davalos, D., Ryu, J.K., Merlini, M., Baeten, K.M., Le Moan, N., Petersen, M.A., Deerinck, T.J., Smirnoff, D.S., Bedard, C., Hakozaki, H., Gonias Murray, S., Ling, J.B., Lassmann, H., Degen, J.L., Ellisman, M.H., Akassoglou, K., 2012. Fibrinogen-induced perivascular microglial clustering is required for the development of axonal damage in neuroinflammation. Nat. Commun. 3, 1227.

Dong, H., Zhang, W., Zeng, X., Hu, G., Zhang, H., He, S., Zhang, S., 2014. Histamine induces upregulated expression of histamine receptors and increases release of inflammatory mediators from microglia. Mol. Neurobiol. 49, 1487–1500.

Dorand, R.D., Barkauskas, D.S., Evans, T.A., Petrosiute, A., Huang, A.Y., 2014. Comparison of intravital thinned skull and cranial window approaches to study CNS immunobiology in the mouse cortex. IntraVital 3, e29728.

Edelson, P.J., Zwiebel, R., Cohn, Z.A., 1975. The pinocytic rate of activated macrophages. J. Exp. Med. 142, 1150–1164.

Feng, D., Nagy, J.A., Hipp, J., Dvorak, H.F., Dvorak, A.M., 1996. Vesiculo-vacuolar organelles and the regulation of venule permeability to macromolecules by vascular permeability factor, histamine, and serotonin. J. Exp. Med. 183, 1981–1986.

Findling, A., Schilling, L., Bultmann, A., Wahl, M., 1994. Computerised image analysis in conjunction with fluorescence microscopy for the study of blood–brain barrier permeability in vivo. Pflugers Arch. 427, 86–95.

Floris, S., Blezer, E.L., Schreibelt, G., Döpp, E., van der Pol, S.M., Schadee-Eestermans, I.L., Nicolay, K., Dijkstra, C.D., de Vries, H.E., 2004. Blood–brain barrier permeability and monocyte infiltration in experimental allergic encephalomyelitis: a quantitative MRI study. Brain 127, 616–627.

Flügel, A., Odoardi, F., Nosov, M., Kawakami, N., 2007. Autoaggressive effector T cells in the course of experimental autoimmune encephalomyelitis visualized in the light of two-photon microscopy. J. Neuroimmunol. 191, 86–97.

Giunti, D., Parodi, B., Cordano, C., Uccelli, A., Kerlero de Rosbo, N., 2013. Can we switch microglia's phenotype to foster neuroprotection? Focus on multiple sclerosis. Immunology 141 (3), 323–339.

Gordon, F.L., Nguyen, K.B., White, C.A., Pender, M.P., 2001. Rapid entry and downregulation of T cells in the central nervous system during the reinduction of experimental autoimmune encephalomyelitis. J. Neuroimmunol. 112, 15–27.

Goverman, J., 2009. Autoimmune T cell responses in the central nervous system. Nat. Rev. Immunol. 9, 393–407.

Greter, M., Heppner, F.L., Lemos, M.P., Odermatt, B.M., Goebels, N., Laufer, T., Noelle, R.J., Becher, B., 2005. Dendritic cells permit immune invasion of the CNS in an animal model of multiple sclerosis. Nat. Med. 11, 328–334.

Hawkins, B.T., Davis, T.P., 2005. The blood–brain barrier/neurovascular unit in health and disease. Pharmacol. Rev. 57, 173–185.

Hendriks, J.J., Teunissen, C.E., de Vries, H.E., Dijkstra, C.D., 2005. Macrophages and neurodegeneration. Brain Res. Brain Res. Rev. 48, 185–195.

Heppner, F.L., Greter, M., Marino, D., Falsig, J., Raivich, G., Hövelmeyer, N., Waisman, A., Rülicke, T., Prinz, M., Priller, J., Becher, B., Aguzzi, A., 2005. Experimental autoimmune encephalomyelitis repressed by microglial paralysis. Nat. Med. 11, 146–152.

Herz, J., Paterka, M., Niesner, R.A., Brandt, A.U., Siffrin, V., Leuenberger, T., Birkenstock, J., Mossakowski, A., Glumm, R., Zipp, F., Radbruch, H., 2011. In vivo imaging of lymphocytes in the CNS reveals different behaviour of naïve T cells in health and autoimmunity. J. Neuroinflammation 8, 131.

Jadidi-Niaragh, F., Mirshafiey, A., 2010. Histamine and histamine receptors in pathogenesis and treatment of multiple sclerosis. Neuropharmacology 59, 180–189.

Juedes, A.E., Ruddle, N.H., 2001. Resident and infiltrating central nervous system APCs regulate the emergence and resolution of experimental autoimmune encephalomyelitis. J. Immunol. 166, 5168–5175.

Kakizoe, E., Kobayashi, Y., Gonda, T., Shimoura, K., Hattori, K., Okunishi, H., 1997. Synergistic interactions between neuropeptide and histamine on the capillary permeability in rat skin: evaluation by reflectance spectrophotometry. Microvasc. Res. 54, 27–34.

Kasper, L.H., Shoemaker, J., 2010. Multiple sclerosis immunology: the healthy immune system vs the MS immune system. Neurology 74 (Suppl. 1), S2–S8.

Kenne, E., Lindbom, L., 2011. Imaging inflammatory plasma leakage in vivo. Thromb. Haemost. 105, 783–789.

Kerfoot, S.M., Long, E.M., Hickey, M.J., Andonegui, G., Lapointe, B.M., Zanardo, R.C., Bonder, C., James, W.G., Robbins, S.M., Kubes, P., 2004. TLR4 contributes to disease-inducing mechanisms resulting in central nervous system autoimmune disease. J. Immunol. 173 (11), 7070–7077.

Kettenmann, H., Hanisch, U.K., Noda, M., Verkhratsky, A., 2011. Physiology of microglia. Physiol. Rev. 91, 461–553.

Kim, J.V., Jiang, N., Tadokoro, C.E., Liu, L., Ransohoff, R.M., Lafaille, J.J., Dustin, M.L., 2010. Two-photon laser scanning microscopy imaging of intact spinal cord and cerebral cortex reveals requirement for CXCR6 and neuroinflammation in immune cell infiltration of cortical injury sites. J. Immunol. Methods 352, 89–100.

Koh, C.S., Gausas, J., Paterson, P.Y., 1993. Neurovascular permeability and fibrin deposition in the central neuraxis of Lewis rats with cell-transferred experimental allergic encephalomyelitis in relationship to clinical and histopathological features of the disease. J. Neuroimmunol. 47, 141–145.

Korn, T., Bettelli, E., Oukka, M., Kuchroo, V.K., 2009. IL-17 and Th17 cells. Annu. Rev. Immunol. 27, 485–517.

Lapilla, M., Gallo, B., Martinello, M., Procaccini, C., Costanza, M., Musio, S., Rossi, B., Angiari, S., Farina, C., Steinman, L., Matarese, G., Constantin, G., Pedotti, R., 2011. Histamine regulates autoreactive T cell activation and adhesiveness in inflamed brain microcirculation. J. Leukoc. Biol. 89, 259–267.

Lassmann, H., Brück, W., Lucchinetti, C.F., 2007. The immunopathology of multiple sclerosis: an overview. Brain Pathol. 17, 210–218.

Linthicum, D.S., Munoz, J.J., Blaskett, A., 1982. Acute experimental autoimmune encephalomyelitis in mice. I. Adjuvant action of *Bordetella pertussis* is due to vasoactive amine sensitization and increased vascular permeability of the central nervous system. Cell. Immunol. 73, 299–310.

Locht, C., Coutte, L., Mielcarek, N., 2011. The ins and outs of pertussis toxin. FEBS J. 278, 4668–4682.

Lodygin, D., Odoardi, F., Schlager, C., Korner, H., Kitz, A., Nosov, M., van den Brandt, J., Reichardt, H.M., Haberl, M., Flugel, A., 2013. A combination of fluorescent NFAT and H2B sensors uncovers dynamics of T cell activation in real time during CNS autoimmunity. Nat. Med. 19, 784–790.

Logothetis, L., Mylonas, I.A., Baloyannis, S., Pashalidou, M., Orologas, A., Zafeiropoulos, A., Kosta, V., Theoharides, T.C., 2005. A pilot, open label, clinical trial using hydroxyzine in multiple sclerosis. Int. J. Immunopathol. Pharmacol. 18, 771–778.

Luo, J., Ho, P., Steinman, L., Wyss-Coray, T., 2008. Bioluminescence in vivo imaging of autoimmune encephalomyelitis predicts disease. J. Neuroinflammation 5, 6.

McGavern, D.B., Kang, S.S., 2011. Illuminating viral infections in the nervous system. Nat. Rev. Immunol. 11, 318–329.

Mi, S., Hu, B., Hahm, K., Luo, Y., Kam Hui, E.S., Yuan, Q., Wong, W.M., Wang, L., Su, H., Chu, T.H., Guo, J., Zhang, W., So, K.F., Pepinsky, B., Shao, Z., Graff, C., Garber, E., Jung, V., Wu, E.X., Wu, W., 2007. LINGO-1 antagonist promotes spinal cord remyelination and axonal integrity in MOG-induced experimental autoimmune encephalomyelitis. Nat. Med. 13, 1228–1233.

Miller, S.D., McMahon, E.J., Schreiner, B., Bailey, S.L., 2007. Antigen presentation in the CNS by myeloid dendritic cells drives progression of relapsing experimental autoimmune encephalomyelitis. Ann. N. Y. Acad. Sci. 1103, 179–191.

Miyata, S., Morita, S., 2011. A new method for visualization of endothelial cells and extravascular leakage in adult mouse brain using fluorescein isothiocyanate. J. Neurosci. Methods 202, 9–16.

Montaner, L.J., da Silva, R.P., Sun, J., Sutterwala, S., Hollinshead, M., Vaux, D., Gordon, S., 1999. Type 1 and type 2 cytokine regulation of macrophage endocytosis: differential activation by IL-4/IL-13 as opposed to IFN-gamma or IL-10. J. Immunol. 162, 4606–4613.

Mostany, R., Portera-Cailliau, C., 2008. A method for 2-photon imaging of blood flow in the neocortex through a cranial window. J. Vis. Exp. 12 (pii 678).

Mues, M., Bartholomäus, I., Thestrup, T., Griesbeck, O., Wekerle, H., Kawakami, N., Krishnamoorthy, G., 2013. Real-time in vivo analysis of T cell activation in the central nervous system using a genetically encoded calcium indicator. Nat. Med. 19, 778–783.

Muller, D.M., Pender, M.P., Greer, J.M., 2005. Blood–brain barrier disruption and lesion localisation in experimental autoimmune encephalomyelitis with predominant cerebellar and brainstem involvement. J. Neuroimmunol. 160 (1–2), 162–169.

Neumann, H., Kotter, M.R., Franklin, R.J., 2009. Debris clearance by microglia: an essential link between degeneration and regeneration. Brain 132, 288–295.

Odoardi, F., Sie, C., Streyl, K., Ulaganathan, V.K., Schlager, C., Lodygin, D., Heckelsmiller, K., Nietfeld, W., Ellwart, J., Klinkert, W.E., Lottaz, C., Nosov, M., Brinkmann, V., Spang, R.,

Lehrach, H., Vingron, M., Wekerle, H., Flugel-Koch, C., Flugel, A., 2012. T cells become licensed in the lung to enter the central nervous system. Nature 488, 675–679.
Olesen, S.P., 1985. A calcium-dependent reversible permeability increase in microvessels in frog brain, induced by serotonin. J. Physiol. 361, 103–113.
Pashenkov, M., Teleshova, N., Link, H., 2003. Inflammation in the central nervous system: the role for dendritic cells. Brain Pathol. 13, 23–33.
Ponomarev, E.D., Shriver, L.P., Maresz, K., Dittel, B.N., 2005. Microglial cell activation and proliferation precedes the onset of CNS autoimmunity. J. Neurosci. Res. 81, 374–389.
Ransohoff, R.M., Engelhardt, B., 2012. The anatomical and cellular basis of immune surveillance in the central nervous system. Nat. Rev. Immunol. 12, 623–635.
Reinke, E.K., Johnson, M.J., Ling, C., Karman, J., Lee, J., Weinstock, J.V., Sandor, M., Fabry, Z., 2006. Substance P receptor mediated maintenance of chronic inflammation in EAE. J. Neuroimmunol. 180, 117–125.
Rothhammer, V., Heink, S., Petermann, F., Srivastava, R., Claussen, M.C., Hemmer, B., Korn, T., 2011. Th17 lymphocytes traffic to the central nervous system independently of alpha4 integrin expression during EAE. J. Exp. Med. 208, 2465–2476.
Saijo, K., Glass, C.K., 2011. Microglial cell origin and phenotypes in health and disease. Nat. Rev. Immunol. 11, 775–787.
Saligrama, N., Noubade, R., Case, L.K., del Rio, R., Teuscher, C., 2012. Combinatorial roles for histamine H1–H2 and H3–H4 receptors in autoimmune inflammatory disease of the central nervous system. Eur. J. Immunol. 42, 1536–1546.
Sallusto, F., Impellizzieri, D., Basso, C., Laroni, A., Uccelli, A., Lanzavecchia, A., Engelhardt, B., 2012. T-cell trafficking in the central nervous system. Immunol. Rev. 248, 216–227.
Saria, A., Lundberg, J.M., Skofitsch, G., Lembeck, F., 1983. Vascular protein linkage in various tissue induced by substance P, capsaicin, bradykinin, serotonin, histamine and by antigen challenge. Naunyn Schmiedeberg's Arch. Pharmacol. 324, 212–218.
Serafini, B., Columba-Cabezas, S., Di Rosa, F., Aloisi, F., 2000. Intracerebral recruitment and maturation of dendritic cells in the onset and progression of experimental autoimmune encephalomyelitis. Am. J. Pathol. 157, 1991–2002.
Siffrin, V., Radbruch, H., Glumm, R., Niesner, R., Paterka, M., Herz, J., Leuenberger, T., Lehmann, S.M., Luenstedt, S., Rinnenthal, J.L., Laube, G., Luche, H., Lehnardt, S., Fehling, H.J., Griesbeck, O., Zipp, F., 2010. In vivo imaging of partially reversible th17 cell-induced neuronal dysfunction in the course of encephalomyelitis. Immunity 33, 424–436.
Sosa, R.A., Murphey, C., Ji, N., Cardona, A.E., Forsthuber, T.G., 2013. The kinetics of myelin antigen uptake by myeloid cells in the central nervous system during experimental autoimmune encephalomyelitis. J. Immunol. 191, 5848–5857.
Stromnes, I.M., Goverman, J.M., 2006. Passive induction of experimental allergic encephalomyelitis. Nat. Protoc. 1, 1952–1960.
Tonra, J.R., Reiseter, B.S., Kolbeck, R., Nagashima, K., Robertson, R., Keyt, B., Lindsay, R.M., 2001. Comparison of the timing of acute blood–brain barrier breakdown to rabbit immunoglobulin G in the cerebellum and spinal cord of mice with experimental autoimmune encephalomyelitis. J. Comp. Neurol. 430, 131–144.
Tsang, A.W., Oestergaard, K., Myers, J.T., Swanson, J.A., 2000. Altered membrane trafficking in activated bone marrow-derived macrophages. J. Leukoc. Biol. 68, 487–494.
Zlokovic, B.V., 2011. Neurovascular pathways to neurodegeneration in Alzheimer's disease and other disorders. Nat. Rev. Neurosci. 12, 723–738.